ACS APPLIED MATERIALS & INTERFACES

Research Article

www.acsami.org

Ag Nanoparticle Decorated Nanoporous ZnO Microrods and Their Enhanced Photocatalytic Activities

Quan Deng,[†] Xiaowei Duan,[†] Dickon H. L. Ng,[‡] Haibin Tang,[†] Yong Yang,[†] Mingguang Kong,[†] Zhikun Wu,[†] Weiping Cai,[†] and Guozhong Wang*[,†]

[†]Key Laboratory of Materials Physics, Anhui Key Laboratory of Nanomaterials and Nanotechnology, Institute of Solid State Physics, Chinese Academy of Sciences, P.O. Box 1129, Hefei 230031, P.R. China

[‡]Department of Physics, The Chinese University of Hong Kong, Shatin, Hong Kong

Supporting Information

ABSTRACT: Nanostructured Ag nanoparticles (Ag-NPs)/nanoporous ZnO micrometer-rods (n-ZnO MRs) have been synthesized by a two-step method. The n-ZnO MRs was initially prepared by solvothermal-assisted heat treatment. The rods had the diameter ranged from 90 to 150 nm and length between 0.5 and 3 μm. They were found to be porous and were composited of ZnO nanopartiles with size of about 20 nm. In the second stage, Ag-NPs with a diameter of 20−50 nm were anchored onto the surface of the as-prepared n-ZnO MRs by a photoreduction method. The Ag-NPs/n-ZnO MRs were evaluated for their ability to degrade methylene blue (MB) solution under visible to ultraviolet (UV) light irradiation. The rate of degradation of the as-prepared Ag-NPs/n-ZnO MRs was more than twice and nearly 5.6 times faster than that of using bare n-ZnO MRs under the UV and solar light irradiation, respectively. The formation of Schottky barriers in the regions between the Ag-NPs and n-ZnO MRs had improved the charge separation and consequently enhanced the efficiency of the degradation process. Moreover, the as-prepared hybrid structure exhibited high photostability, and 98% of degradation efficiency could be maintained even after being used five times. This endurance was attributed to the retardation of photocorrosion of ZnO as a result of the low concentration of surface defects in the as-prepared n-ZnO MRs. It also minimized the surface defects of the as-prepared n-ZnO MRs and consequently further inhibited the photocorrosion of ZnO when the deposited Ag-NPs were much more inclined to combine with the chemisorbed oxygen.

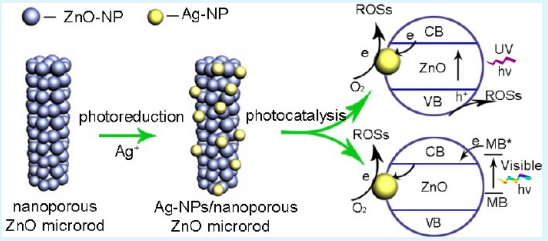

KEYWORDS: *Ag nanoparticles, ZnO micrometer-rods, solvothermal method, photoreduction, photocatalytic activities*

1. INTRODUCTION

Semiconductor photocatalysis has attracted a great deal of attentions due to their wide application to environmental remediation, especially for organic pollutants removal.[1,2] As an important semiconductor photocatalyst, zinc oxides (ZnO) have been widely studied for environmental remediation.[3] However, ZnO is a wide band gap (3.37 eV) semiconductor with inevitable shortcomings for photocatalysis-based applications. Such photocatalysts only active under UV irradiation but often with low photocatalytic efficiency and high rate of photocorrosion. Also, nanosized ZnO materials are normally unstable, easy to be agglomerated and difficult to recovery after use.

The poor resistance to photocorrosion and rapid performance decay of the nanosized ZnO materials are directly resulted from the agglomeration due to the poor structural stability. Therefore, preventing the nanosized structure from agglomeration is the key for preserving the high photocatalytic activity of nanosized photocatalysts. In this regard, assembling nanosized structures onto microstructures has been proven to be effective.[4−6] This is because that the nano/microstructures possess an overall dimension in micrometers with nanosized units. The assembled nanosized units are stabilized to ensure a superior structural stability so the agglomeration is minimized. Also, the photocatalytic activity of such nano/microstructured configurations can be preserved due to the presence of the nanosized units. It has been reported that the photocorrosion mainly occurred at the surface defect sites of ZnO.[7,8] Thus the synthesis of ZnO with good crystalline quality would effectively minimize the surface defects hence improve the photocorrosion properties. The above information suggests that ZnO-based photocatalysts with high stability and photocatalytic performance could be achieved by fabricating high crystalline ZnO having nano/microstructures.

It has been well demonstrated that the photocatalytic efficiency of ZnO can be effectively enhanced by means of surface modification with noble metal nanoparticles.[9−15] The enhanced photocatalytic performance could be attributed to the special metal−semiconductor interface, allowing for the establishment of the Schottky Barrier to facilitate the charge

Received: August 17, 2012
Accepted: October 23, 2012
Published: October 23, 2012

separation.[16,17] This may also be attributed to the enhanced adsorption capability and kinetic properties introduced by the specific interactions at the metal−semiconductor interface[18] and increased productivity of active hydroxyl radicals due to the presence of high surface concentration of hydroxyls resulted from the interaction of metal nanoparticles with the semiconductor.[19] Different noble metals have been modified onto the ZnO surface in nanoparticle forms to improve the photocatalytic activity.[9−15] Amongst them, Ag-NPs modified ZnO has shown significantly improved photocatalytic degradation performance toward organic contaminants.[14,15,19−24] The Ag-NPs has been successfully decorated onto ZnO with different geometries/morphologies such as nanofibers,[21] rods,[14,25,26] and spheres.[19,20] All resultant Ag-NPs decorated ZnO photocatalysts reported to date exhibit an enhanced photocatalytic performance toward the degradation of organic contaminants such as methyl orange, rhodamine B, and orange G.[14,15,19,23,24]

Herein, we report a uniquely configured Ag-NPs decorated nanoporous ZnO micrometer-rods heterostructure (Ag-NPs/n-ZnO MRs) with enhanced UV and solar light photocatalytic activities and improved stability. The n-ZnO MRs composed of ZnO nanoparticles with high specific surface area (20.87 $m^2 g^{-1}$) and bi-pore-size-distribution were fabricated via a facile solvothermal-assisted heat treatment method developed by our group.[27,28] The Ag-NPs were decorated onto the n-ZnO MRs by solar light photoreduction of Ag ions. The UV and solar light photocatalytic performance, and photostability of the as-prepared Ag-NPs/n-ZnO MRs were evaluated using methylene blue (MB) as a probe compound.

Additionally, our as-prepared hybrid structure displayed better photostability in UV and solar light region than the reported Ag-NPs/ZnO heterostructures.[29] We found that the content of Ag-NPs deposited on the ZnO rods had a significant effect on the photocatalytic efficiency of the product. Our results demonstrated that the nanostructured Ag-NPs/n-ZnO MRs exhibited enhanced photocatalytic performance and high stability to reuse in degradation of organic dye MB, which might provide a good candidate material for organic pollutants remediation.

2. EXPERIMENTAL SECTION

2.1. Materials. All chemicals were of analytical grade and used as received without further purification, unless otherwise stated. Zinc acetate dihydrate ($C_4H_6O_4Zn{\cdot}2H_2O$) was purchased from Guangfu Fine Chemical Research Institute (Tianjin, China). Oxalic acid dihydrate ($C_2H_2O_4{\cdot}2H_2O$) and ethylene glycol ($(CH_2OH)_2$) were obtained from Suyi Chemical Reagent Co., Ltd (Shanghai, China). Silver nitrate ($AgNO_3$) was purchased from Guangfu Technology Development Co., Ltd (Tianjin, China).

2.2. Samples Preparation. The n-ZnO MRs constructed with ZnO nanoparticles were synthesized via a solvothermal-assisted heat treatment method.[27,28] To obtain the precursor zinc oxalate, 25 mmol $C_4H_6O_4Zn{\cdot}2H_2O$ and 25 mmol $C_2H_2O_4{\cdot}2H_2O$ were added into 40 ml of absolute ethyl alcohol under constant stirring until the mixture became gel and, then, transferred into a Teflon liner stainless-steel autoclave (70 mL). The sealed autoclave was heated under a constant temperature of 80 °C for 5 h. After cooling to room temperature, the precipitate was washed repeatedly with deionized water and then dried at 60 °C for 1 h. This intermediate product was annealed at 450 °C for 2 h, and the ZnO nanoparticles were constructed ZnO micrometer-rods with good quality crystalline were obtained. The sample was labelled n-ZnO MRs.

A solar light photoreduction method was used to decorate Ag-NPs onto the surface of the as prepared n-ZnO MRs. $AgNO_3$ was dissolved in ethylene glycol. Solutions containing different concentrations of $AgNO_3$ (0.05, 0.07, and 0.1 mol L^{-1}) were prepared. An 800 mg portion of the as-prepared n-ZnO MRs were placed in 24 mL of each reaction solution. The reaction solution was irradiated for 15 min in a photochemical reaction instrument under continuous stirring. A 500 W xenon lamp with main wavelength of 365−720 nm was used as the solar light resource for photoreduction. The precipitate was separated from the reaction solution by centrifugation at 3000 rpm for 3 min. The product was washed with ethanol and rinsed with distilled water before being heated at 60 °C for 8 h. Three Ag-NPs/n-ZnO MRs photocatalysts were obtained by using 0.05, 0.07, and 0.1 mol L^{-1} of $AgNO_3$ glycol solutions, and they were labelled as ZnOA-1, ZnOA-2, and ZnOA-3, respectively.

2.3. Characterization. The crystalline structures of the products were identified by X-ray diffraction analysis (XRD, Philips X pert PRO) using Ni-filtered monochromatic Cu Kα radiation at 40 keV and 40 mA. Field emission scanning electron microscope (FESEM, Sirion 200 FEG) employing an accelerating voltage of 10.00 or 15.00 kV, and transmission electron microscopy (TEM, JEOL-2010, 200 kV) with an energy dispersive X-ray spectrometer (EDX) were used to characterize the morphologies and elemental distributions. The surface area of the products was determined by nitrogen adsorption (Micrometrics ASAP 2020M). X-ray photoelectron spectroscopy (XPS) was performed by a Thermo ESCALAB 250 photoelectron spectrometer with Al Kα X-rays as the excitation source. The UV-Vis absorption spectra were recorded by spectrophotometer (CARY-5E). The content of deposited Ag-NPs in the Ag-NPs/n-ZnO MRs photocatalysts was measured by an inductive coupled plasma optical emission spectrometer (ICP, ICP6300, Thermo Fisher Scientific). The UV-Vis diffuse-reflection spectra were measured on a UV-Vis-near-IR spectrometer (UV3600-MPC3100). Room-temperature fluorescent characterization was carried out by a confocal microprobe Raman system (LABRAM-HR, France) using an excitation wavelength of 325 nm. Raman scattering spectra of the samples were obtained by using a spectrometer (NEXUS, USA). The 532 nm line of an Ar-ion laser served as excitation source.

2.4. Evaluation of Photocatalytic Performance. MRs (20 mg Ag-NPs/n-ZnO) were added into 80 mL of 1.25×10^{-5} mol L^{-1} MB solution. A 300W UV lamp with maximum emission at 365 nm was used as UV light source. A 500 W xenon lamp of which main wavelength lies in 365−720 nm was used as the solar light source for sunlight photocatalysis. The above mixture solution was irradiated in a photochemical chamber under continuous stirring. Before irradiation, the solution was stirred for 30 min in the dark to reach an adsorption−desorption equilibrium between the photocatalyst and MB. At certain time intervals, 3 mL solution was drawn out each time and centrifuged at 7000 rpm for 2 min to get clear liquid. The quantitative determination of MB was performed by measuring its intensity of the absorption peak with a UV−vis spectrophotometer. Comparative experiments of degradation MB by using n-ZnO MRs and the ZnOA-1, ZnOA-2, and ZnOA-3 samples were also carried out.

3. RESULTS AND DISCUSSION

3.1. Structure and Morphology. Figure 1 shows the XRD patterns of the as-prepared bare n-ZnO MRs and the Ag-NPs/n-ZnO MRs with different Ag contents (ZnOA-1, ZnOA-2, and ZnOA-3). The peaks of typical hexagonal wurtzite structure of ZnO (JCPDS card no. 36-1451) are observed from all samples. For those Ag decorated samples, three additional peaks (marked with * in Figure 1) can be assigned to the fcc Ag peaks (JCPDS card no. 04-0783). It is observed that the intensities of the Ag peaks namely (111), (200), and (220) increase with the increased Ag content. In order to quantify the deposited Ag-NPs content, the Ag-NPs/n-ZnO MRs samples were dispersed in distilled water (5 mL) and eluted by adding nitric acid, respectively. The Ag contents of the elution solutions were determined by the ICP, and the calculated results are shown in Table 1.

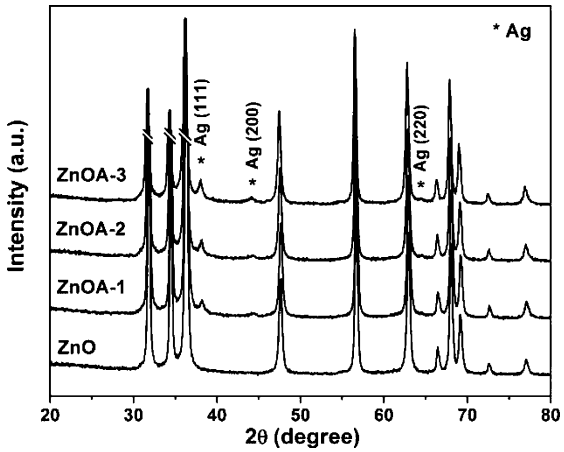

Figure 1. XRD patterns of the as-prepared bare n-ZnO MRs and Ag-NPs/n-ZnO MRs decorated with different amounts of Ag-NPs.

Table 1. Ag Contents of Ag-NPs/n-ZnO MRs Samples

Ag-NPs/n-ZnO MRs	$AgNO_3$ (mol L^{-1})	Ag (wt %)
ZnOA-1	0.05	1.22
ZnOA-2	0.07	1.66
ZnOA-3	0.1	2.16

The morphologies of the as-prepared n-ZnO MRs and ZnOA-2 are shown in Figure 2. The SEM image of the as-prepared n-ZnO MRs showed that the sample was rod (Figure 2a) with diameter of about 90−150 nm and a length of about 0.5−3 μm. The TEM image (inset in Figure 2a) showed that the ZnO rod was highly porous (illustrated by the open circles in the inset) and composed of ZnO nanoparticles with an average dimension of ∼20 nm. Further annealing would produce thicker ZnO porous micrometer-rods with a diameter of about 0.5−1.5 μm. The growth of the rods was the result of combining nearby rods (shown in Supporting Information Figure S1). To further clarify the specific surface area and pore size distribution of the n-ZnO MRs, nitrogen adsorption/desorption isotherms were obtained measured and the results are presented in Supporting Information Figure S2a. According to the Brunauer−Deming−Deming−Teller classification,[30] the sample exhibited the type IV isotherm, indicating that they were mesoporous. We had also derived the pore size distribution of the n-ZnO MRs (see inset in Supporting Information Figure S2a) based on the desorption data. We found that the pore size distribution was not uniform (mainly around 3 to 30 nm), and there were some obvious bi-pore size distribution characteristic. These results were consistent with the results of TEM analysis (see inset in Figure 2) and the results of our previous work.[27]

After the decoration of the Ag-NPs on the n-ZnO MRs, the morphology of the n-ZnO MRs was retained as shown in Figure 2b for the ZnOA-2 sample. Further structural characterization of the ZnOA-2 with TEM is shown in Figure 3. Figure 3a showed that the product had a typical nanoporous rod-like structure, and the Ag-NPs with a diameter of 20-50 nm were found attaching onto the surface of n-ZnO MRs. HRTEM image (Figure 3b) at the Ag-ZnO interface (marked with a circle in Figure 3a) revealed the interplanar spacing of about 0.28 nm, corresponding to the (100) plane of ZnO, while the interplanar spacing of 0.235 nm could be assigned to the (101) plane of Ag. The spatial distribution of different compositional

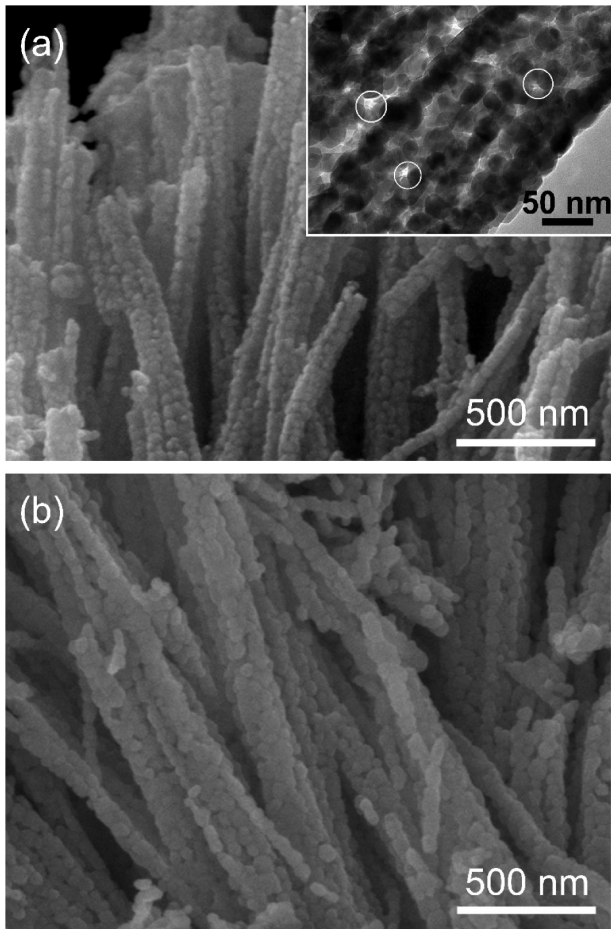

Figure 2. SEM images of (a) the as-prepared n-ZnO MRs (the inset shows the high-magnification view of TEM) and (b) ZnOA-2 sample.

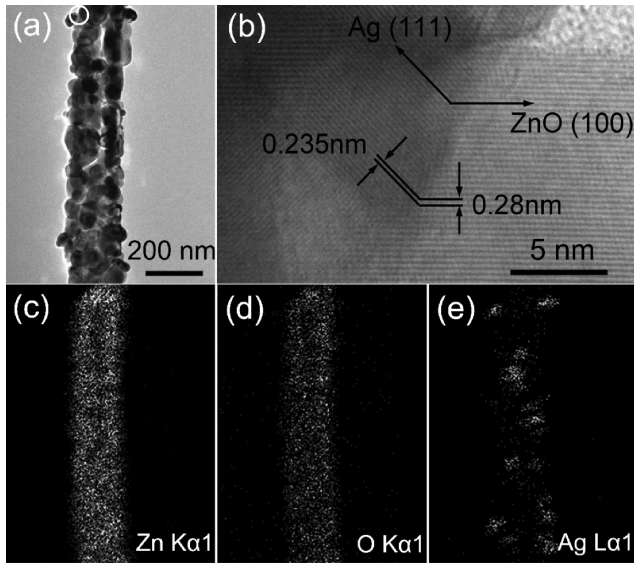

Figure 3. (a) TEM image of the as-prepared ZnOA-2 sample; (b) HRTEM image of the area marked with a circle in part a; (c−e) elemental mapping images of elemental Zn, O and Ag, respectively.

elements of the ZnOA-2 sample were clarified by the elemental mapping of Zn Kα1 edge (8631 eV), O Kα1 edge (525 eV), and Ag Lα1 edge (2984 eV), respectively, as shown in Figure 3c−e. The Ag contents were found to be distributed in a

discontinued cluster form corresponding to the observed Ag-NPs locations by the TEM image shown in Figure 3a. At the same time, the determined Zn and O contents were found to be evenly distributed throughout the entire rod, as expected. Thus we confirmed that the Ag-NPs had been successfully deposited onto the surface of the n-ZnO MRs, and the original morphology of the n-ZnO MRs has not been altered. Moreover, compared with the bare ZnO micrometer-rods, the specific surface area and pore size distribution of ZnOA-2 (see in Supporting Information Figure S2b) had no obvious changes (detailed discussed in part S2).

3.2. Chemical Composition of Ag-NPs/n-ZnO MRs. The XPS analysis was carried out to investigate the chemical composition of the ZnOA-2 sample as shown in Figure 4. The

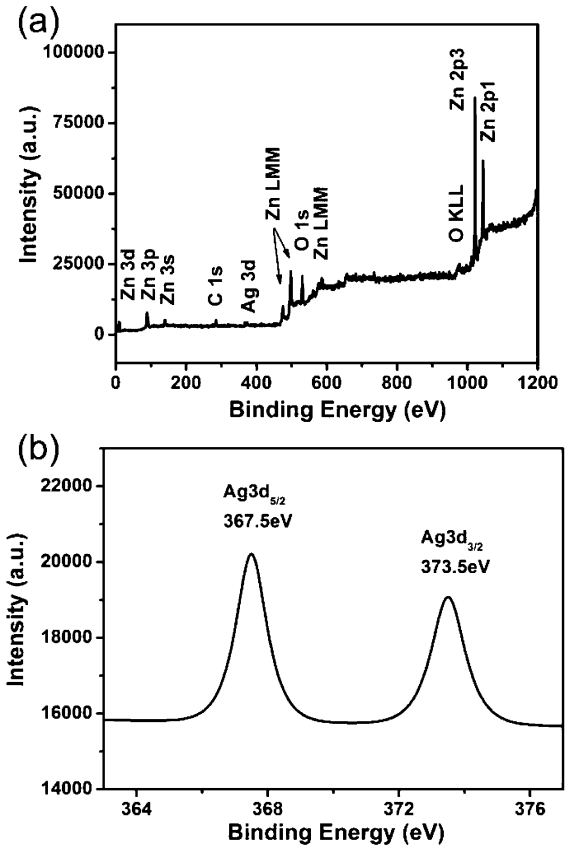

Figure 4. (a) XPS spectra of the as-prepared ZnOA-2 and (b) Ag 3d spectra.

binding energies in the XPS spectra were calibrated using C 1s (284.8 eV). There were no peaks for other elements except Zn, O, Ag, and C observed from the full XPS spectra of Figure 4a, which further confirmed that Ag-NPs had been successfully deposited onto the surface of the n-ZnO MRs. The presence of C came mainly from the carbon dioxide adsorbed on the surface of the sample from the air. Figure 4b is the high-resolution spectra of Ag in the ZnOA-2, where the Ag $3d_{5/2}$ peak appeared at a binding energy of 367.4 eV and the splitting of the 3d doublet was 6.0 eV, indicating the metallic nature of silver.[31] The Ag $3d_{5/2}$ and Ag $3d_{3/2}$ peaks shifted obviously to the lower binding energies compared with the standard values (about 368.2 and 374.2 eV for bulk Ag,[31] respectively), which should be attributed to the transfer of electrons from Ag-NPs to n-ZnO MRs at the interfaces. These results were in agreement with the observations made by other works.[14,20−22] It was evident from these results that the Ag-NPs/n-ZnO MRs consisted of Ag and ZnO.

3.3. Raman Analysis and Optical Properties. To evaluate the crystalline quality and the amount of defects, Raman analysis was performed. Raman spectra (RS) are sensitive to crystallization, structural disorder, and defects in micro and nanostructures. The RS results illustrated that the hexagonal wurtzite structured ZnO belonged to the space group C_{6v},[4] of which the Raman-active modes were A_1, E_1, and $2E_2$.[32] Among these, A_1 and E_1 were polar and split into two transverse optical (TO) and longitudinal optical (LO) phonons. The E_2 mode was nonpolar optical phonon mode, composed of a low and a high frequency. The Raman spectra of the n-ZnO MRs and Ag-NPs/n-ZnO MRs with different Ag-NPs contents in the wavenumber range 80−650 cm^{-1} at room temperature are shown in Figure 5a and Supporting

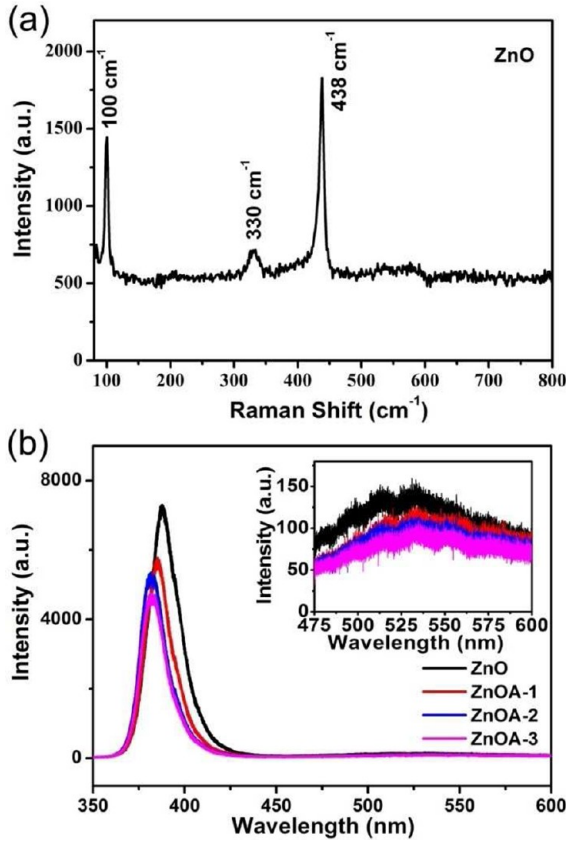

Figure 5. (a) Raman spectra of the as-prepared n-ZnO MRs and (b) PL spectra of the as-prepared n-ZnO MRs and Ag-NPs/n-ZnO MRs.

Information Figure S3, respectively. Three vibration peaks could be observed at 100, 330, and 437 cm^{-1} in Figure 5a. The two strong peaks at 100 and 437 cm^{-1} corresponded to the E_2 mode of ZnO hexagonal wurtzite structure,[33] and the peak at 330 cm^{-1} was attributed to the $3E_{2H}-E_{2L}$ multiphonon vibration.[32] The E_1 (LO) mode, associated with the formation of oxygen deficiency, interstitial Zn, or the free charge carrier,[34] was barely observed. Therefore, the appearance of a high intensity and dominated E_2 mode and almost no E_1 mode in the Raman spectrum indicated that the as-prepared n-ZnO MRs were of high quality crystalline with little structural defects. After decorating Ag-NPs, the fundamental phonon

dx.doi.org/10.1021/am301682g | ACS Appl. Mater. Interfaces 2012, 4, 6030−6037

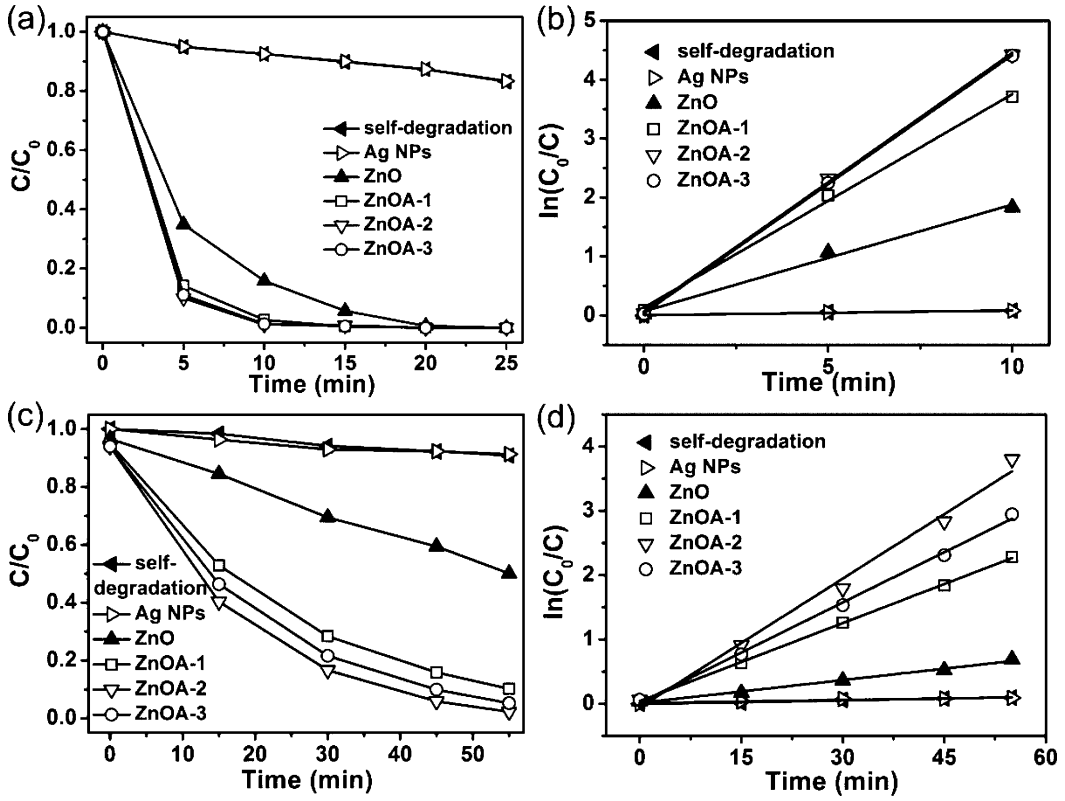

Figure 6. Photocatalytic activity and kinetics of the as-prepared Ag-NPs, n-ZnO MRs, and Ag-NPs/n-ZnO MRs for degradation of MB: (a and b) under UV irradiation; (c and d) under solar light irradiation.

modes of wurtzite ZnO decrease significantly and a broad band around 225 cm^{-1} was observed for the three Ag-NPs/n-ZnO MR photocatalysts (see Supporting Information Figure S3). The broad band was attributed to the $\nu(Ag-O_2)$ of the molecular oxygen species chemisorbed on the defects of metallic Ag,[35] which would be further discussed in the section on the PL spectra.

Figure 5b shows the room-temperature PL spectra of the as-prepared bare n-ZnO MRs and three Ag-NPs/n-ZnO MRs. A strong UV emission peaks round 387 nm and a negligible green band (500−550 nm) were observed in the PL spectra. The UV emission could be assigned to the near-band-edge emission of the wide band gap of ZnO.[36] The green emission was the most common defect emission in the nanostructured ZnO, attributed to the defect state which was located at the surface of nanostructured ZnO,[36] i.e. the singly ionized oxygen vacancy in ZnO,[37] oxygen vacancies, and zinc interstitials.[38] Therefore, the presence of sharp and strong UV emission and the very weak green emission in the PL spectrum of the as-prepared n-ZnO MRs constructed with ZnO nanoparticles implied that there was a low concentration of surface defects in the highly crystallized ZnO rods,[39] which was in agreement with the results obtained by Raman analysis. It was also observed that with the content increasing of Ag-NPs, the intensity of both UV emission and green emission of the Ag-NPs/n-ZnO MRs photocatalysts decrease. The intensity decreasing of the UV emission indicated the reduction of electron-hole recombination.[23] It was because those Ag-NPs deposited on the surface of the ZnO rods would act as traps to capture the photo-generated electrons and hindered the recombination of electron-hole pairs. Theoretically, more Ag-NPs implied a higher electron-hole pairs separation ability.[19] The decreased intensity in green emission indicated that the deposition of Ag-NPs onto the defect sites of ZnO had reduced the surface defects in Ag-NPs/n-ZnO MRs.[40] This was also in accordance with the results obtained in the Raman analysis. The diffuse-reflectance spectra of the as-prepared ZnO and Ag-NPs/n-ZnO MRs were shown in Supporting Information Figure S4. Two prominent absorption bands were observed in the region between 200 and 800 nm. The absorption edge located around 389 nm was assigned to the absorption of ZnO semiconductor, while the maximum absorption band located at around 445 nm attributed to the characteristic absorption of surface plasmon resulting from the metallic Ag-NPs in the Ag/ZnO heterostructure.[41,42] It was also indicated that the Ag-NPs/n-ZnO MRs consist of Ag and ZnO.[14]

3.4. Photocatalytic Activity. The photcatalytic performances in UV and solar light regions were investigated via the degradation of MB, which a typical cationic organic pollutant usually discharged by the textile industry after used. The photocatalytic activity and kinetics of the as-prepared Ag-NPs, n-ZnO MRs, and Ag-NPs/n-ZnO MRs for degradation of MB under UV and solar light irradiation were presented in Figure 6. A control solution without sample was also presented in the same figure for comparison purpose. Figure 6a showed the degradation rate of MB under UV irradiation without photocatalyst (control group) and using the as-prepared Ag-NPs, n-ZnO MRs, and Ag-NPs/n-ZnO MRs modified with different Ag contents, where C was the concentration of MB remaining in the solution after irradiation time t, and C_0 was the initial concentration at $t = 0$. The self-degradation of MB (when no sample was used) was less than 17% under high pressure mercury lamp irradiation for 25 min. It was observed that the degradation of MB by using only Ag-NPs was not obvious, and

the Ag-NPs/n-ZnO MRs displayed higher photocatalytic efficiency than that of n-ZnO MRs. It took almost 20 min for n-ZnO MRs to completely degrade MB, while less than 15 min was needed when the ZnOA-1 was used. Moreover, the degradation of MB using ZnOA-2 and ZnOA-3 took only about 10 min. The photocatalysts degradation kinetic reaction could be described by pseudo-first-order kinetics,[15,20] $\ln(C_0/C) = kt$, where k was a pseudo-first-rate kinetic constant and t was irradiation time. In this work, the squares of linear correlation coefficients (R^2) were all more than 0.98 (see Tables 2 and 3),

Table 2. Reaction Rate Constant (k) for Photocatalytic Degradation of MB under UV Irradiation[a]

UV	n-ZnO MRs	ZnOA-1	ZnOA-2	ZnOA-3
k/min^{-1}	0.18122	0.36216	0.43923	0.43806
R^2	0.98343	0.99624	0.99891	0.99986

[a] R^2 represents the square of correlation coefficient of kinetic linear fitting.

Table 3. Reaction Rate Constant (k) for Photocatalytic Degradation of MB under Solar Light Irradiation[a]

solar light	n-ZnO MRs	ZnOA-1	ZnOA-2	ZnOA-3
k/min^{-1}	0.01184	0.04043	0.06676	0.05204
R^2	0.98861	0.99961	0.98691	0.99714

[a] R^2 represents the square of correlation coefficient of kinetic linear fitting.

thus the photodegradation of MB could be considered as a pseudo-first-order reaction in kinetics and the slope of the linear curve could be considered as the rate constant k. The variations in $\ln(C_0/C)$ as a function of irradiation time were given in Figure 4b. The calculated k value for the as-prepared n-ZnO MRs and Ag-NPs/n-ZnO MRs photocatalysts (ZnOA-1, ZnOA-2, and ZnOA-3) were listed in Table 2. We also found that the k value of the ZnOA-1 was double of the value that obtained from the n-ZnO MRs. It also revealed that the k values obtained from ZnOA-2 and ZnOA-3 were higher than that obtained from ZnOA-1, confirming the enhancement effect of Ag-NPs.

The photocatalytic activity and kinetics of the as-prepared Ag-NPs, bare n-ZnO MRs, and Ag-NPs/n-ZnO MRs for degradation of MB under solar light irradiation are presented in Figures 6c and d. The calculated k values for the as-prepared n-ZnO MRs and Ag-NPs/n-ZnO MRs are listed in Table 3. The control group result showed that the self-degradation of MB was less 10% in the entire irradiation process. The ZnOA-2 with an Ag of 1.66 wt % showed the most superior photocatalytic performance, of which k was 5.6 times larger than that of n-ZnO MRs. With the weight percentage of Ag increased from 0 to 1.66, the photocatalytic efficiency and k had been increased. However, the photocatalytic efficiency and k decreased when the weight percentage increased from 1.66 to 2.26. The results further demonstrated that the amounts of Ag-NPs had a significant impact on the Ag-NPs/n-ZnO MRs' photocatalytic activity. When the weight percentage of Ag-NPs was optimal, it was thermodynamically possible that the Ag-NPs acted as an electron well, and the electrons on the surface of n-ZnO MRs could effectively move toward Ag-NPs. However, some Ag-NPs might act as the recombination centres and inhibited the photocatalytic activity of the Ag-NPs/n-ZnO MRs samples. Similar results were also found by some other works.[43,44]

3.5. Photostability. To investigate the stability of photocatalytic performance in UV and solar light region, the ZnOA-2

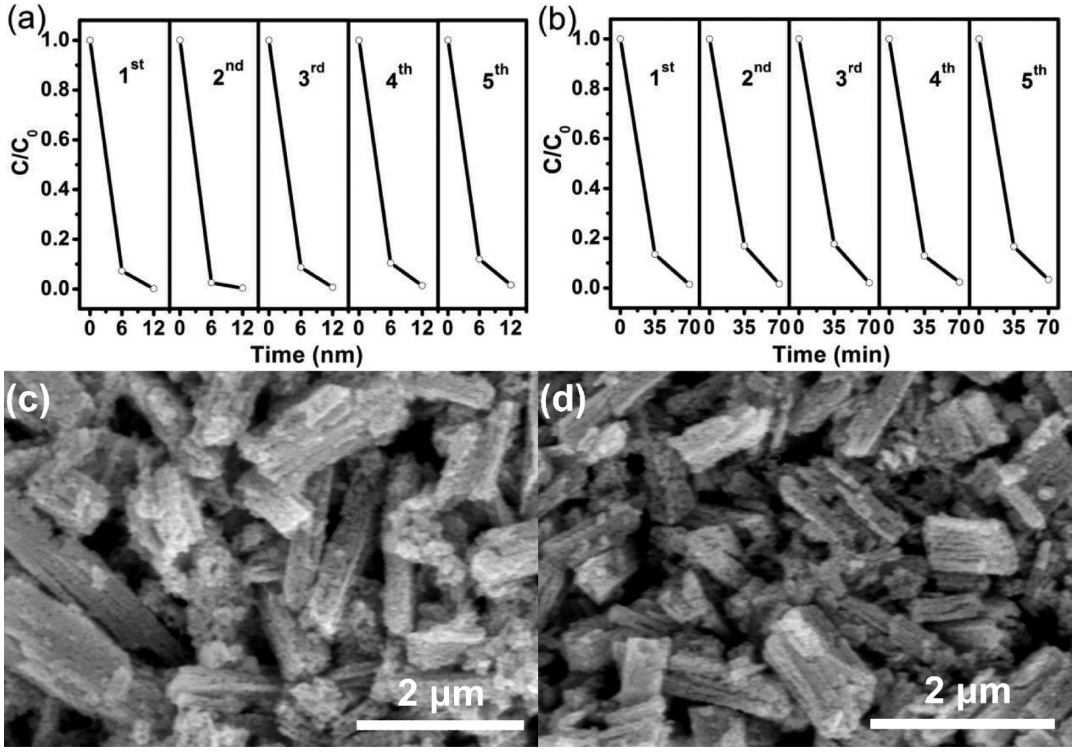

Figure 7. Five photocatalytic degradation cycles of MB using ZnOA-2 under (a) UV, and (b) solar light irradiation, and the FESEM images of ZnOA-2 sample which had been reused after five cycles under (c) UV and (d) solar light irradiation, respectively.

was used to degrade MB dye in five repeated cycles, and the results are shown in Figure 7. It was noteworthy that the photocatalytic performance of the ZnOA-2 exhibited effective photostability under UV (Figure 7a) and solar light irradiation (Figure 7b), where the photocatalytic efficiency reduced only by 1.45% and 1.91% after five cycles, respectively. Two possible reasons were responsible for the favorable photostability as follows. First, the micro/nanostructure photocatalysts possessed both advantages of nano (the highly activity) and micrometer-sized (the structural stability) materials.[4,6] It could be observed that the reused ZnOA-2 retained the original structure with a few attached particles (Figures 7c and d), the SEM image of ZnOA-2 sample after being used for five times under UV and solar light irradiation, respectively. Secondly, the superior crystalline quality of the n-ZnO MRs via annealing at 450 °C for 2 h and the Ag-NPs deposited on the defect sites of the ZnO rods significantly reduced the amount of surface defects in the photocatalyst and effectively inhibit the pthoto-corrosion, resulting in the improvement of photo-stability in photocatalyst.[7,8]

3.6. Mechanisms in Enhancing Photocatalytic Activity. The mechanisms of the enhanced photocatalytic activity of the photocatalyst modified with noble metal have been proposed by others.[19,22,43−53] The degradation of MB over Ag-NPs/n-ZnO MRs under UV and solar light irradiation could be illustrated in Scheme 1. The enhanced photocatalytic

Scheme 1. Schematic Diagram to Illustrate the Process of Photosensitized Degradation of MB by Using Ag-NPs/n-ZnO MRs under UV and Solar Light Irradiation

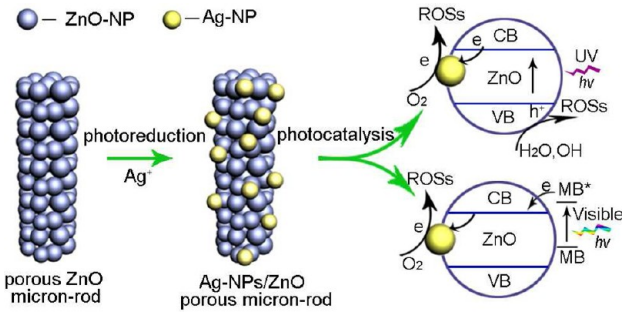

performance in UV region was attributed to the formation of the Schottky barriers at metal-semiconductor interface between the Ag-NPs and the n-ZnO MRs, which improved the segregation of charges and prevented the charge recombination.[22,43−45,47] The Ag-NPs/n-ZnO MRs photocatalysis under UV irradiation involved multiple steps including the formation of the Schottky barriers at metal-semiconductor interaction; excitation of ZnO micrometer-rods by UV light; generation of electron-hole pairs; generation of reactive oxidative species (ROSs); and mineralization of the organic compounds by ROSs.[19,46] For the photocatalysis under solar light irradiation, besides the enhancement in UV region, the adsorbed MB would also be photoactivated by the visible light (shown in Scheme 1), followed by electron transfer from the excited MB (MB*) to the conduction band of ZnO.[46,49,50,52,53] The electrons on the ZnO surface were subsequently trapped by the Ag-NPs, which separated the $MB^{\bullet+}$ and electron, preventing the recombination process.[48] Moreover, the surface plasma resonance of Ag-NPs excited by the solar light improved the excitation of surface electrons and the transfer of interfacial electrons.[43,45,47] Separated electrons might then be consumed by the oxygen molecules dissolved in the solution to generate various ROSs, thus promoting the photocatalysis.[51]

In this work, the unique structural characteristics of the Ag-NPs/n-ZnO MRs are the key to achieve the superior photocatalytic activity and stability (see Scheme 1). The high crystalline ZnO NPs of 20 nm and Ag-NPs of 20−50 nm are responsible for the high photocatalytic activity, while the microstructure of the n-ZnO MRs improve the stability.[4,54] Also, the n-ZnO MRs constructed with ZnO NPs possess larger specific surface area than that of micrometer-rods, favorable for high photocatalytic efficiency. Additionally, the superior crystalline quality of the annealed ZnO rods with significantly reduced the surface defect sites improves the photocorrosion resistance and photostability.

4. CONCLUSIONS

In summary, the Ag-NPs/n-ZnO MRs composing of ZnO nanoparticles had been successfully fabricated via the photoreduction of Ag ions to Ag-NPs onto the surface of the ZnO nanoparticles constructed micrometer-rods fabricated via a solvothermal-assisted heat treatment method. The as-prepared Ag-NPs/n-ZnO MRs had shown significant structure-enhanced photocatalytic activity toward MB degradation under UV, especially under the solar light irradiation. The enhanced photocatalytic activity and significantly improved photostability could be attributed to the unique nano/miroconfigured structure, the superior crystallinity of the ZnO rods, and the decorated Ag-NPs. The Ag-NPs deposited on the ZnO surface act as the electron wells to promote the charge separation and the plasmatic effect of the deposited Ag-NPs enhance the photocatalytic performance in visible region.

■ ASSOCIATED CONTENT

Supporting Information

Some additional figures and discussion are provided in the Supporting Information, including SEM image, pore size distribution (the corresponding discussion), and Raman and UV−vis diffuse-reflection spectra of the as-prepared samples. This material is available free of charge via the Internet at http://pubs.acs.org.

■ AUTHOR INFORMATION

Corresponding Author

*E-mail: gzhwang@issp.ac.cn.

Notes

The authors declare no competing financial interest.

■ ACKNOWLEDGMENTS

This work was supported by the National Basic Research Program of China (Grant No. 2013CB934303), the Natural Science Foundation of China (Grant No. 51072199), and Special Foundation of President of Hefei Institutes of Physical Science, the Chinese Academy of Sciences.

■ REFERENCES

(1) Hoffmann, M. R.; Martin, S. T.; Choi, W. Y.; Bahnemann, D. W. *Chem. Rev.* **1995**, *95*, 69−96.
(2) Mills, A.; LeHunte, S. *J. Photochem. Photobiol. A: Chem* **1997**, *108*, 1−35.
(3) Meng, M.; Lai, Y. L.; Yu, Y. F. *Appl. Catal. B: Environ.* **2010**, *100*, 491−501.

(4) Lu, F.; Cai, W. P.; Zhang, Y. G. *Adv. Funct. Mater.* **2008**, *18*, 1047−1056.
(5) Wang, Y. Q.; Wang, G. Z.; Wang, H. Q.; Cai, W. P.; Zhang, L. D. *Chem. Commun.* **2008**, 6555−6557.
(6) Li, J.; Wang, G. Z.; Wang, H. Q.; Tang, C. J.; Wang, Y. Q.; Liang, C. H.; Cai, W. P.; Zhang, L. D. *J. Mater. Chem.* **2009**, *19*, 2253−2258.
(7) Fu, H. B.; Xu, T. G.; Zhu, S. B.; Zhu, Y. F. *Environ. Sci. Technol.* **2008**, *42*, 8064−8069.
(8) Kislov, N.; Lahiri, J.; Verma, H.; Goswami, D. Y.; Stefanakos, E.; Batzill, M. *Langmuir* **2009**, *25*, 3310−3315.
(9) Zeng, H. B.; Liu, P. S.; Cai, W. P.; Yang, S. K.; Xu, X. X. *J. Phys. Chem. C* **2008**, *112*, 19620−19624.
(10) Jing, L. Q.; Wang, D. J.; Wang, B. Q.; Li, S. D.; Xin, B. F.; Fu, H. G.; Sun, J. Z. *J. Mol. Catal. A: Chem.* **2006**, *244*, 193−200.
(11) Wang, Q.; Geng, B. Y.; Wang, S. Z. *Environ. Sci. Technol.* **2009**, *43*, 8968−8973.
(12) Xu, Y. G.; Xu, H.; Li, H. M.; Xia, J. X.; Liu, C. T.; Liu, L. *J. Alloys Compd.* **2011**, *509*, 3286−3292.
(13) Jing, L. Q.; Cai, W. M.; Sun, X. J.; Hou, H.; Xu, Z. L.; Du, Y. G. *Chin. J. Catal.* **2002**, *23*, 336−340.
(14) Zheng, Y. H.; Zheng, L. R.; Zhan, Y. Y.; Lin, X. Y.; Zheng, Q.; Wei, K. M. *Inorg. Chem.* **2007**, *46*, 6980−6986.
(15) Li, X. Z.; Li, F. B. *Environ. Sci. Technol.* **2001**, *35*, 2381−2387.
(16) Linsebigler, A. L.; Lu, G. Q.; Yates, J. T. *Chem. Rev.* **1995**, *95*, 735−758.
(17) Tada, H.; Teranishi, K.; Inubushi, Y.; Ito, S. *Langmuir* **2000**, *16*, 3304−3309.
(18) Lu, W. W.; Gao, S. Y.; Wang, J. J. *J. Phys. Chem. C* **2008**, *112*, 16792−16800.
(19) Height, M. J.; Pratsinis, S. E.; Mekasuwandumrong, O.; Praserthdam, P. *Appl. Catal. B: Environ.* **2006**, *63*, 305−312.
(20) Lai, Y. L.; Meng, M.; Yu, Y. F. *Appl. Catal. B: Environ.* **2010**, *100*, 491−501.
(21) Lin, D. D.; Wu, H.; Zhang, R.; Pan, W. *Chem. Mater.* **2009**, *21*, 3479−3484.
(22) Gu, C. D.; Cheng, C.; Huang, H. Y.; Wong, T. L.; Wang, N.; Zhang, T. Y. *Cryst. Growth Des.* **2009**, *9*, 3278−3285.
(23) Georgekutty, R.; Seery, M. K.; Pillai, S. C. *J. Phys. Chem. C* **2008**, *112*, 13563−13570.
(24) Zheng, Y. H.; Chen, C. Q.; Zhan, Y. Y.; Lin, X. Y.; Zheng, Q.; Wei, K. M.; Zhu, J. F. *J. Phys. Chem. C* **2008**, *112*, 10773−10777.
(25) Ren, C. L.; Yang, B. F.; Wu, M.; Xu, J. A.; Fu, Z. P.; Lv, Y.; Guo, T.; Zhao, Y. X.; Zhu, C. Q. *J. Hazard. Mater.* **2010**, *182*, 123−129.
(26) Chen, T. W.; Zheng, Y. H.; Lin, J. M.; Chen, G. N. *J. Am. Soc. Mass. Spectrom.* **2008**, *19*, 997−1003.
(27) Duan, X. W.; Wang, G. Z.; Wang, H. Q.; Wang, Y. Q.; Shen, C.; Cai, W. P. *CrystEngComm* **2010**, *12*, 2821−2825.
(28) Yang, L.; Wang, G. Z.; Tang, C. J.; Wang, H. Q.; Zhang, L. *Chem. Phys. Lett.* **2005**, *409*, 337−341.
(29) Yang, Z. M.; Zhang, P.; Ding, Y. H.; Jiang, Y.; Long, Z. L.; Dai, W. L. *Mater. Res. Bull.* **2011**, *46*, 1625−1631.
(30) Sing, K. S. W.; Everett, D. H.; Haul, R. A. W.; Moscou, L.; Pierotti, R. A.; Rouquerol, J.; Siemieniewska, T. *Pure Appl. Chem.* **1985**, *57*, 603−619.
(31) Gang, L.; Anderson, B. G.; van Grondelle, J.; van Santen, R. A. *Appl. Catal. B: Environ.* **2003**, *40*, 101−110.
(32) Damen, T. C.; Porto, S. P. S.; Tell, B. *Phys. Rev.* **1966**, *142*, 570−&.
(33) Xing, Y. J.; Xi, Z. H.; Xue, Z. Q.; Zhang, X. D.; Song, J. H.; Wang, R. M.; Xu, J.; Song, Y.; Zhang, S. L.; Yu, D. P. *Appl. Phys. Lett.* **2003**, *83*, 1689−1691.
(34) Zeng, J. N.; Low, J. K.; Ren, Z. M.; Liew, T.; Lu, Y. F. *Appl. Surf. Sci.* **2002**, *197*, 362−367.
(35) Millar, G. J.; Metson, J. B.; Bowmaker, G. A.; Cooney, R. P. *J. Chem. Soc., Faraday Trans.* **1995**, *91*, 4149−4159.
(36) Djurisic, A. B.; Leung, Y. H. *Small* **2006**, *2*, 944−961.
(37) Vanheusden, K.; Warren, W. L.; Seager, C. H.; Tallant, D. R.; Voigt, J. A.; Gnade, B. E. *J. Appl. Phys.* **1996**, *79*, 7983−7990.
(38) Liu, X.; Wu, X. H.; Cao, H.; Chang, R. P. H. *J. Appl. Phys.* **2004**, *95*, 3141−3147.
(39) Wu, J. J.; Liu, S. C. *J. Phys. Chem. B* **2002**, *106*, 9546−9551.
(40) Xie, W.; Li, Y. Z.; Sun, W.; Huang, J. C.; Xie, H.; Zhao, X. J. *J. Photochem. Photobio. A: Chem.* **2010**, *216*, 149−155.
(41) Zhao, Y.; Jiang, Y. J.; Fang, Y. *Spectrochim. Acta. A* **2006**, *65*, 1003−1006.
(42) Zhang, L.; Dou, Y. H.; Gu, H. C. *J. Colloid Interf. Sci.* **2006**, *297*, 660−664.
(43) Sung-Suh, H. M.; Choi, J. R.; Hah, H. J.; Koo, S. M.; Bae, Y. C. *J. Photochem. Photobio. A: Chem.* **2004**, *163*, 37−44.
(44) Chuang, H. Y.; Chen, D. H. *Nanotechnology* **2009**, 20.
(45) Herrmann, J. M.; Tahiri, H.; AitIchou, Y.; Lassaletta, G.; GonzalezElipe, A. R.; Fernandez, A. *Appl. Catal. B: Environ.* **1997**, *13*, 219−228.
(46) Wu, T. X.; Liu, G. M.; Zhao, J. C.; Hidaka, H.; Serpone, N. *J. Phys. Chem. B* **1998**, *102*, 5845−5851.
(47) Zhao, G.; Kozuka, H.; Yoko, T. *Thin Solid Films* **1996**, *277*, 147−154.
(48) Xiong, Z. G.; Zhang, L. L.; Ma, J. Z.; Zhao, X. S. *Chem. Commun.* **2010**, *46*, 6099−6101.
(49) Hagfeldt, A.; Gratzel, M. *Chem. Rev.* **1995**, *95*, 49−68.
(50) Kamat, P. V. *Chem. Rev.* **1993**, *93*, 267−300.
(51) Ryu, J.; Choi, W. *Environ. Sci. Technol.* **2004**, *38*, 2928−2933.
(52) Zhao, D.; Chen, C.; Wang, Y.; Ma, W.; Zhao, J.; Rajh, T.; Zang, L. *Environ. Sci. Technol.* **2008**, *42*, 308−314.
(53) Rehman, S.; Ullah, R.; Butt, A. M.; Gohar, N. D. *J. Hazard. Mater.* **2009**, *170*, 560−569.
(54) Wang, X. B.; Cai, W. P.; Lin, Y. X.; Wang, G. Z.; Liang, C. H. *J. Mater. Chem.* **2010**, *20*, 8582−8590.